# Electronic Hong Ou Mandel interferences to unveil the 2/3 fractional quantum Hall edge channel dynamics


## Authors:

A. De [1†], C. Boudet[1†], M. Kapfer[1], I. Farrer[2], D. A. Ritchie[3], P. Roulleau[1] and D.C. Glattli[1*],

**Affiliations:**

[1] SPEC, CEA, CNRS, Université Paris-Saclay, CEA Saclay, 91191 Gif sur Yvette Cedex France

[2]School of Electrical & Electronic Engineering, University of Sheffield, Mappin Street, S1 3JD, UK

[3]Cavendish Laboratory, University of Cambridge, J.J. Thomson Avenue, Cambridge CB3 0HE, UK.

† these two authors equally contributed to the work.


## Supplementary Information:



**A1. Sample characteristics and fabrication:** samples are 2DEGs with electrons confined at the interface of high mobility epitaxially grown GaAs/GaAlAs heterojunctions at 90 nm below the surface. The low temperature zero field mobility is $300 m^2 s^{-1} V^{-1}$ and the electron density is $n_s = 1{,}11.10^{15} m^{-2}$. For this density, the bulk filling factor $\nu_B = 2/5$ corresponds to a magnetic field of ≈11.2 Tesla. Ohmic contacts are realized by evaporating 125 nm Au, 60 nm Ge, 4 nm Ni followed by annealing at 470°C. A shallow mesa etching (H3PO4 phosphoric acid, time 4 minutes) defines the sample. The QPC gates are realized by e-beam lithography, see

Fig.S1 for a SEM image of the sample used. The edge channel length between each contacts and the center of the QPC is about 18µm. .

.

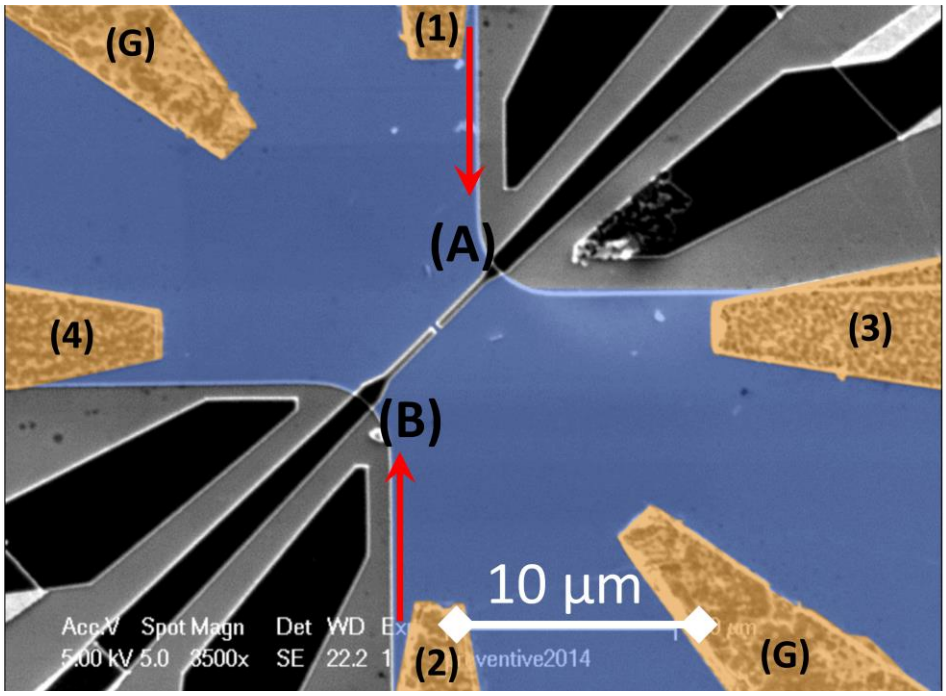


**Figure S1-1: SEM view of the sample used.** Yellow areas are ohmic contacts, blue aeras denote the un-etched part of 2DEG mesa. A 10um black bar indicates the scale. (A) and (B) denote the probable location of the mixing tunneling point defects coupling the co-propagating channels at ν=2 and 3 discussed in part C2 of the supplementary material

**A2. Measurement set-up:** an ultra-low temperature cryo-free dilution refrigerator with a 22 mK base temperature from CryoConcept is used as in[40,44,51] . It is equipped with a dry superconducting coil able to reach 14.5 Tesla. Ultra-low-loss dc-40GHz microwave cables bring the room temperature microwave excitation from a 20GHz AnaPico APMSXXG-4 4 channel RF source to a Printed Circuit Board (PCB). The RF power of the microwave source, given in the main text is attenuated by fixed 60dB cold attenuators and extra losses in the cryogenic coaxial cables. Coplanar waveguides designed by CST microwave Studio$^{R}$ etched on the PCB bring the two radiofrequency excitations to ohmic contact (1) and (2) of the sample, see Fig.1(a) and Fig.S1-1. Noise measurements are obtained by separately converting the transmitted and reflected current fluctuations into voltage fluctuations at contact (3) and (4) respectively in parallel to a R-L-C resonant circuit tuned to 2,2 MHz frequency and bandwidth $\approx$ 150 kHz, with R=20kOhms. Note that an effective resonant circuit resistance $R_{eff.} = RR_L/(R + R_L) \approx 6.5$kOhms is found instead of 20kOhms due to inductance loss, giving a shunt resistance $R_L = (L2\pi f_0)^2/r$ in parallel to R, where r=15 Ohms is the series resistance of the inductance. Finally, the Q factor of the RLC resonant circuit is given by the ratio of the parallel resistance $R_{eff}//R_{Hall}$ to the characteristic impedance $\sqrt{\frac{L}{C}}$, where $R_{Hall}$ is the Hall resistance of the sample. The voltage fluctuations are amplified by two home-made cryogenic amplifiers with 0.22 nV/Hz$^{1/2}$ input noise at low temperature, followed by low noise room temperature amplifiers. The amplified fluctuations are passed through Chebyshev filters and

then sent to a fast 20Ms/s digital acquisition card (ADLink 9852) while a PC provides real-time computation of the cross-correlation spectrum. Absolute Noise calibration is done by recording the equilibrium Johnson Nyquist noise when varying the temperature from 20mK to 200mK. Differential Conductance measurements giving the transmission and reflection are made by applying a low frequency AC voltage, frequency 270Hz, and μV amplitude voltage to contact (1) and sending the amplified AC voltage from contacts (3) and (4) to two Lock-in amplifiers. The low frequency measurement accuracy is mostly limited by the large 1/f noise of the cryogenic HEMT (white noise cross-over at ≈1MHz). The shot noise accuracy is limited by the input white noise of the amplifier and time averaging. For $\nu_B$=2/3, the 20kOhm resistor and the effective RLC parallel resistance $R_{eff}$=6.5kOhms in parallel with the bulk Hall resistance converts the input noise of 220pV/Hz$^{1/2}$ into 2.510$^{-27}$A$^2$/Hz equivalent current noise power. Using cross-correlation and noise averaging during the typical measurement time $\tau_m$ =3s with ≈150kHz effective detection bandwidth around the 2.3 MHz RLC resonant frequency, the accuracy of a raw noise data point is +/- 3.7 10$^{-30}$A$^2$/Hz. Longer measurement times can be used to increase the accuracy.

**A3 Lorentzian voltage pulses:**

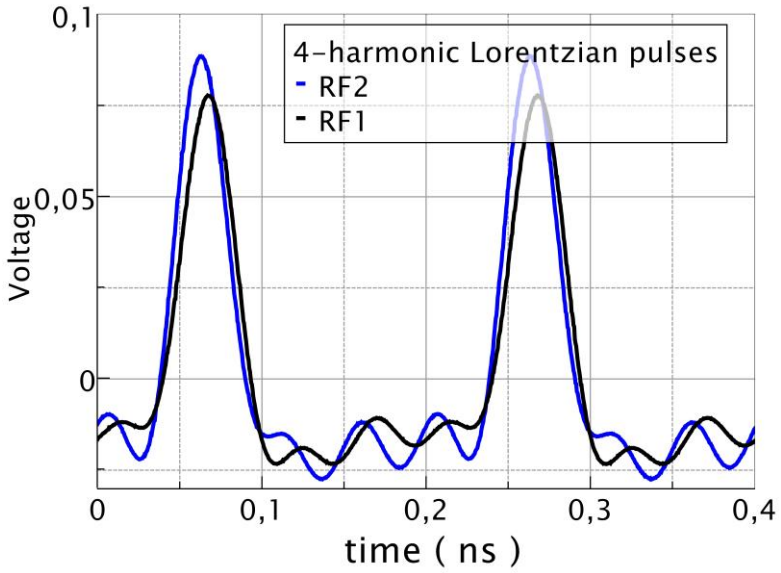


**Figure S1-3: generation of Lorentzian voltage pulses.** The pulses generated at the output of the room temperature Anapico RF source by a combination of four harmonics[54,55,56] of 5-20GHz with appropriate amplitudes and then splitted into the two signal shown in the figure. The black (blue) curve is the excitation sent to contact (1) and (2) respectively. Both are attenuated by 60dB and additional few dB RF-loss along the cryogenic coaxes. Small difference are due to residual imbalance in the RF power splitter used to separate the signal into two.

Figure S1-3 shows the pulses injected towards the upper left and lower right ohmic contacts (1) and (2). As only the first four harmonics of the Lorentzian pulse are used, the pulse show no DC component. The small oscillmations in the voltage signal the lack of harmonics higher than the fourth. Note that the lack of DC component of the pulses.

**B: the 2/3 edge channel dynamics model:**

**Model:**

We use the model developed in Ref.[32] . Starting with the following equation of motion:

$$\frac{\partial}{\partial t}\vec{I} = -\sigma C^{-1}\frac{\partial}{\partial x}\vec{I} - -\sigma C^{-1} g \sigma^{-1}\vec{I} \qquad \text{(S1)},$$

where $\vec{I} = \begin{pmatrix} I_1 \\ I_2 \end{pmatrix}$ with $I_{1(2)}(x,t)$ denoting the current in outer(inner) channel at time t and point x, $\sigma = \sigma_q \begin{pmatrix} 1 & 0 \\ 0 & -1/3 \end{pmatrix}$ accounts for the channel conductances, $g = g\begin{pmatrix} 1 & -1 \\ -1 & 1 \end{pmatrix}$ describes the inter-channel tunneling conductance and $C = \begin{pmatrix} C_1 + C_X & -C_X \\ -C_X & C_2 + C_X \end{pmatrix}$ the interaction with $C_{1(2)}$ the outer(inner) channel self-capacitance per unit length and $C_X$ the inter-channel capacitance per unit length[32,57]. We seek a solution of the form $\begin{pmatrix} I_1(x,t) \\ I_2(x,t) \end{pmatrix} = \begin{pmatrix} I_1 \\ I_2 \end{pmatrix} \exp i(kx - \omega t)$. The local electro-chemical potential expressed in units of voltage are related to the local current via $V_1(x,t) = I_1(x,t)/\sigma_q$ and $V_2(x,t) = -3I_2(x,t)/\sigma_q$.

We can make connection with the abelian field theory of FQHE edges described by the Lagrangian[22,24]:

$$L = \frac{1}{4\pi}[\partial_T \varphi^T K \partial_x \varphi - \partial_x \varphi^T V \partial_x \varphi] \qquad \text{(S2)}$$

With $\varphi=(V_1,V_2)$ and $K = \sigma_q \sigma^{-1}$ and $V = \sigma_q C^{-1}$. The chosen parameters $C_X$=0.4nF/m, $C_1=C_2$=0.1nF/m correspond to a K-F-P initial renormalization parameter[22] $\Delta$=1.109 close to renormalization fixed point $\Delta$=1 leading to a quasi-charge and quasi-neutral modes. The

solutions are given by diagonalization of equation (S1). Here we recall the results obtained in Ref.[32]. An important dimensionless parameter is

$$\boldsymbol{\xi(\omega) = \xi_O \left(1 + \frac{f_{C.o}}{f}\right)} \tag{S3}$$

with $\xi_0$=$C_X$/($C_1$+3$C_2$) and $\boldsymbol{f_{C.0.} = \frac{1}{2\pi}\frac{e^2}{2hC_X l_{eq.}}}$.

Solution (I): Charge mode.

Let us define, as done in Ref.[32] , the convenient intermediate variable: $\boldsymbol{X(\xi) = \sqrt{1 - 4\xi + (4\xi)^2}}$. With this notation, the charge mode solution corresponds to a wavevector $k_I$=$k'_I$+i$k''_I$ given by:

$$\boldsymbol{k_I = \frac{\omega}{2\sigma_q}\left[C_1\left(1 - 2\xi + X(\xi)\right) - 3C_2\left(1 + 2\xi - X(\xi)\right)\right]} \tag{S4}$$

With voltage components on the outer and inner channel $\begin{pmatrix} \mathbf{1} \\ \mathbf{-3I_I} \end{pmatrix}$, with: $\boldsymbol{I_I = \frac{-2\xi}{1+4\xi+X(\xi)}}$.

The following graph shows the variations of the charge mode phase velocity $v_c$=$\omega/k'_I$, the charge mode attenuation length $1/k''_I$ and the inner to outer channel voltage ratio of the charge mode.

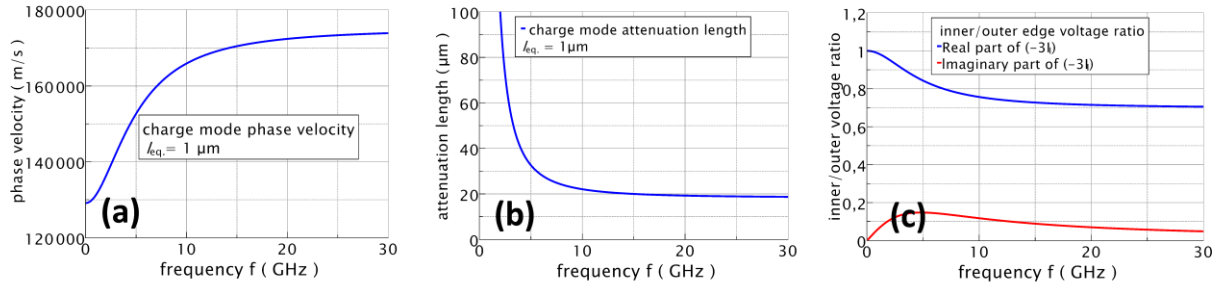


**Figure S2: computed charge mode characteristics for a typical charge relaxation length of $l_{eq.}$=1 µm. (a)** phase velocity versus frequency. The velocity shows a significant variation around the cross-over frequency $f_{C.O.}$=7.7 GHz for $l_{eq.}$=1 µm. This is expected to lead to dispersive effects**. (b)** the charge mode attenuation is shown to be infinite at zero frequency and to remain quite large >20µm at high frequency. **(c)** inner/outer voltage ratio versus frequency. At low frequency the mode is a pure charge mode ($V_1$(x,t)=$V_2$(x,t)) while at high frequency it

is expected to be a quasi-charge mode with few 10% imbalance between the inner and outer voltages.

Solution (II): Neutral mode.

The neutral mode solution corresponds to a wavevector $k_{II}=k'_{II}+ik''_{II}$ given by:

$$\boldsymbol{k_{II}} = \frac{\boldsymbol{\omega}}{\boldsymbol{2\sigma_q}}\left[\boldsymbol{C_1}\left(\boldsymbol{1-2\xi-X(\xi)}\right)-\boldsymbol{3C_2}\left(\boldsymbol{1+2\xi+X(\xi)}\right)\right] \qquad \text{(S5)}$$

With components of the current on the outer and inner channel are $\begin{pmatrix} \boldsymbol{I_{II}} \\ \boldsymbol{1} \end{pmatrix}$, with: $\boldsymbol{I_{II}} = \frac{\boldsymbol{1+4\xi-X(\xi)}}{\boldsymbol{-2\xi}}$.

The following graph shows the variations of the neutral mode phase velocity $v_n=\omega/k'_{II}$, the neutral mode attenuation length $1/k''_{II}$ and the outer to inner current ratio of the neutral mode.

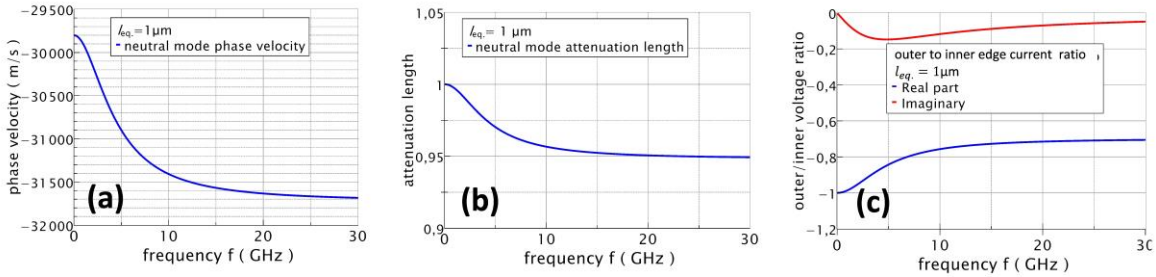


**Figure S3: neutral mode characteristics for $l_{eq.}$=1µm. (a)** the neutral mode velocity is negative, i.e. the neutral mode propagate upstream. Note the frequency dispersion around $f_{C.O.}$ as also observed for the charge mode**. (b) attenuation length: the neutral mode exponential decay occurs over a length smaller than** $l_{eq.}$ and reaches $l_{eq.}$ in the DC limit**. (c)** the negative value signals a pure neutral mode with opposite current $I_1(x,t)= - I_2(x,t)$ at low frequency, while at high frequency the mode is only quasi-neutral.

The next step is to calculate the AC potential at the middle of the QPC point x=L, given the applied AC potential $V_{01}$ at the upper left injecting ohmic contact, point x=0, where x denotes the curvilinear abcissa along the edge channel. A similar calculation can be done when injecting from the lower right contact. To proceed, we remark that the neutral mode cannot propagate as the attenuation is stronger than $\exp(-L/l_{eq.})=2.\ 10^{-6}$ and we are left to only consider the charge mode. We use the charge mode scattering amplitude of current derived in equation (22) of Ref.[32], and the inner to outer amplitude ratio $I_I$ to calculate the inner channel voltage $V_2(t,L)$ at the QPC. We find:

$$V_2(t,L) = RE[(-3)V_{01}(1-I_1I_2)I_1 e^{i(k'_1L-2\pi ft)}e^{-k''_1L} \qquad \text{(S6)}$$

With the complex $k_I$ given by equation S4. This leads to the calculated AC amplitude reduction shown in figure 2(d) of the main text and expected for various values of $l_{eq.}$ .

We can also calculate the deformation of periodic Lorentzian pulses injected at contact (1) after their 20µm propagation towards the QPC. This is shown in figure S4 for various $l_{eq.}$. The Lorentzian repetition frequency is 5GHz and the full width at mid-height is 36ps. For simplicity and direct use of equation S6, the Lorentzian is approximated by the sum of the first four harmonics at 5, 10, 15, and 20 GHz. The truncation is responsible for the small oscillations observed in the black dashed curves in figures S4(a-d) which show the injected pulses

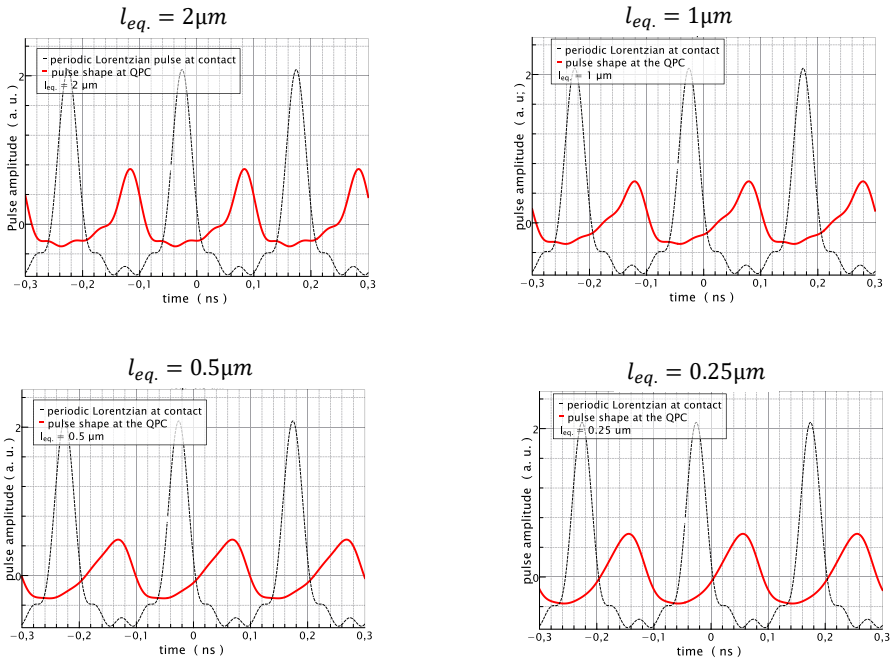


**Figure S4: Lorentzian pulse deformation for various $l_{eq.}$=2 to 0.25µm.** The black dashed curve represent the 4-harmonics periodic Lorentzian injected at the ohmic contact (1) and the red solid curves the inner channel voltage calculated at the QPC, propagation length of 20µm. The periodicity is 5GHz (period 0.2ns) and the full width at mid height 36ps. The voltage calculated at the QPC shows asymmetric deformation due to dispersive effects and amplitude reduction as well as broadening due to damping by inter-channel tunneling. These trends increase while reducing the charge equilibration length as shown in figure (b to d) for $l_{eq.}$=1, 0.5 and 0.25µm.

The next figure S5 shows the calculated expect HOM noise variations for two different values of $l_{eq.}$. The black dashed curve correspond to an unrealistic value of 100µm and the red open circle to 0.5µm. The latter is well fitted by a sinewave variation (dashed red curve) indicating the loss of high frequency components of the original Lorentzian pulses, while the former cannot be fitted by a sinewave (dashed blue curve) as for 100µm equilibration one would expect the Lorentzian pulses not to be deformed. To calculated the HOM noise we use to identical pulses injected with a relative time-delay τ at contact (1) and (2). The calculation is

done for weak backscattering giving Poissonian shot noise and follows the approach developed in Ref.[55] for levitons.

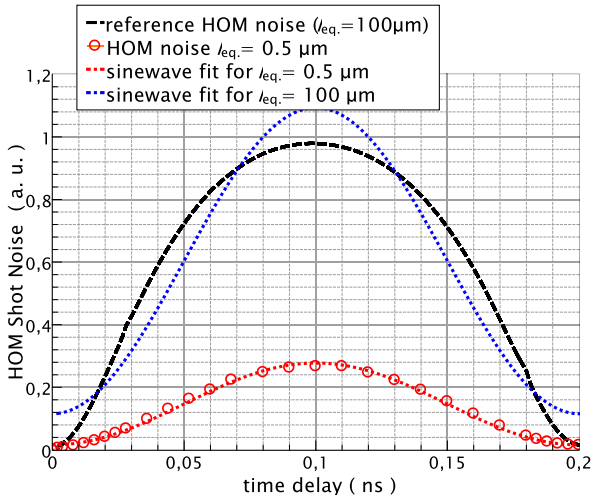


**Figure S5: calculated HOM shot noise for indistinguishable** Lorentzian charge pulses colliding at the QPC for $l_{eq.}$ =100µm (black dashed curve) and $l_{eq.}$ =0.5µm red open circle). The blue and red dotted curves are best sinewave fit for both $l_{eq.}$ values**.**

## C: additional data:

## C1. PASN shot noise at 17.05 GHz:

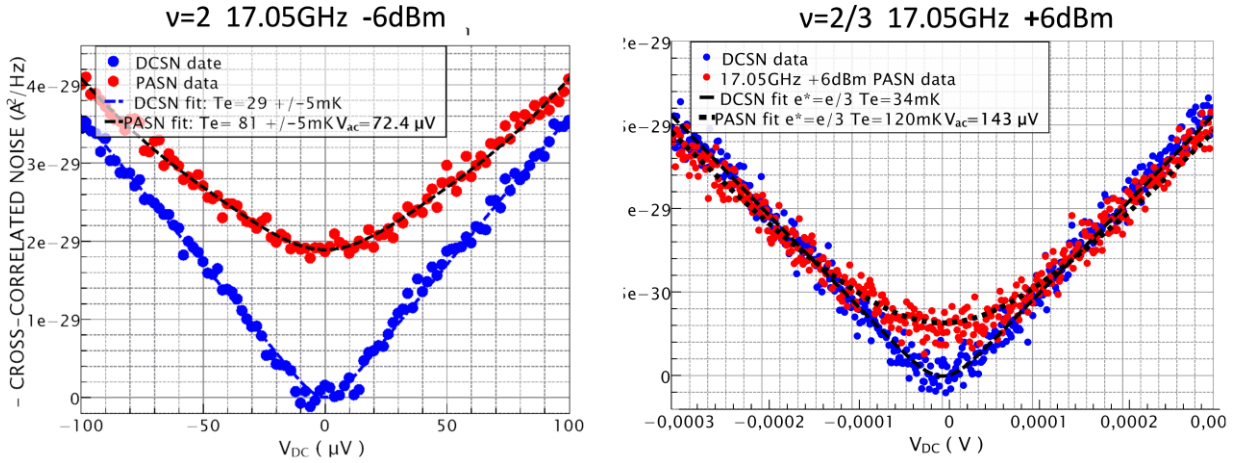


**Figure S6: PASN determination of charge mode attenuation at 17.05GHz.** The procedure is similar to that done in figure 2(a) and (b), main text, for 15.3GHz RF drive. Left graph: filling factor ν=2, the RF source power is -6dBm. Blue circles points: DCSN, red circles PASN. The dashed lines are fits using $T_e$=29+/-1.5mK and, 81+/-4mK and $V_{ac}$(ν=2)=74+/-1.5µV for DCSN and PASN respectively. The higher PASN temperature is due to RF heating. From this we estimate de AC voltage applied on contact (1) as: 74+/-3µV<$V_{01}$<~88+/-4µV. Right graph: same but for ν=2/3 and +6dBm RF power. The

fits give $T_e$=34+/-2mK and, $T_e$=120+/-10mK and $V_{ac}(\nu=2/3)$=143+/-3μV for DCSN and PASN respectively. The charge mode attenuation from the contact to the QPC is : 0.40+/-0.02 $<V_{ac}(\nu=2/3)/4V_{01}<$0.483+/-0.03. From the computed attenuation shown figure 2(d), main text, this confirms the estimation 1μm ≤ $l_{eq.}$ ≤ 2μm.

## C2. HOM Shot Noise analysis at ν=2

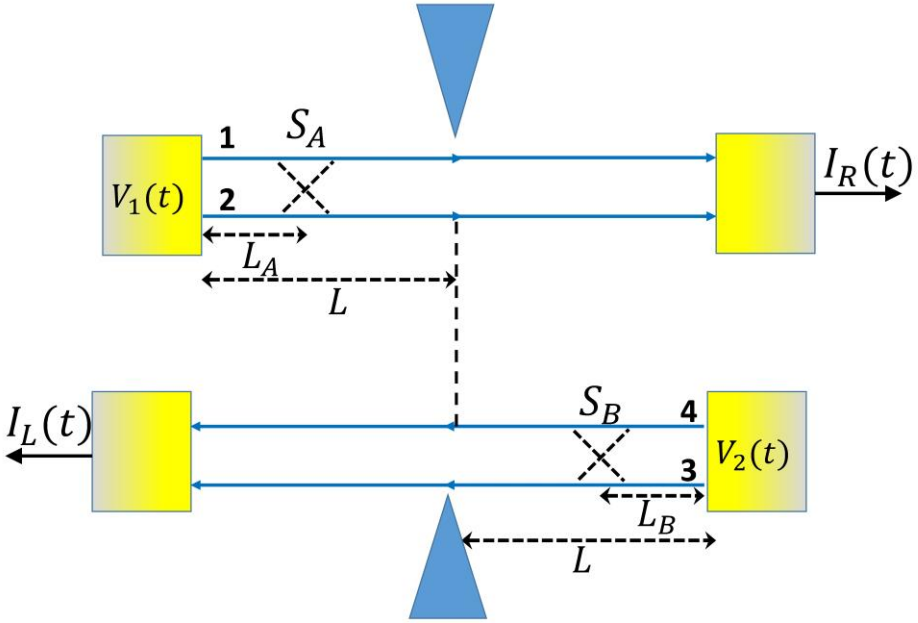


**Figure S7:** schematic representation of discrete inter-channel tunneling points located on opposite side of the QPC

Assuming perfect propagation along the input edge channels, the Lorentzian pulses sent at opposite contacts (1) and (2) should give a single HOM dip versus the time delay (modulo the period T=200ps). However, We observe a split central dip and an additional dip around τ=100ps (mod. T).

Here we explain the reason for the multiple dips. We refer to the work of Refs[51,52,53] suggesting local tunnel mixing points along the co-propagating edge at ν=2 (and also 3). Because the single particle drift velocities of the outer and inner channels are different, we expect several propagation times for excited charge pulses to reach the QPC. In case of a unique tunnel mixing point (A) in the left input edge there will be a propagation time for a quasiparticle emitted in the inner channel and remaining in this channel with probability $T_A=(1-R_A)$ different from than the time for a quasiparticle emitted in the outer edge channel and transferred to the inner channel with probability $R_A=1-T_A$. As similar mixing may occur on the opposite input edge at a point (B), see figure S7.

A probable location of the mixing point is at the transition between the ungated at gated edge channels denoted as (A) and (B) in figure S1. Indeed, a right angle turn is known to mix edge channel[58] . For ν=3 this leads to mix the channel belonging to the first and second Landau levels[58]. For ν=2, the Rashba spin orbit, due to the perpendicular electric field confining electrons at the interface of the GaAs/GaAlAs heterojunction[59], is expected to mix the spin while the momentum is forced to make a right angle change of direction[59,60,61,62,63]. We expect that the time-domain electronic HOM shot noise would represent the combination of several

HOM dips representing the collision of various charge pulses weighted by the mixing probabilities. More explicitly, according to[52], for two discrete tunneling mixing points, each localized on the input arm of the opposite input edge channels, the expected HOM noise is given by:

$$S_I(\tau) = RD[T_A T_B S_{HOM}(\Delta_{24}) + T_A R_B S_{HOM}(\Delta_{23}) + R_A T_B S_{HOM}(\Delta_{14}) + R_A R_B S_{HOM}(\Delta_{13})] + R^2[R_A T_A S_{HOM}(\Delta_{12}) + T_B T_B S_{HOM}(\Delta_{34})] \quad \text{(S7)}$$

With R=1-D the reflection probability at the QPC. The last two terms are τ-independent and correspond to the partitioning of electron between inner and outer edge channels in each input arm with $\Delta_{12}=L_A(1/v_1-1/v_2)$ and $\Delta_{34}=L_B(1/v_3-1/v_4)$ where $L_{A(B)}$ is the distance between the mixing point A (B) from the ohmic contact 1 (2). Their contribution gives an offset in the HOM noise. The first four time are τ-dependent terms and correspond to a discrete sum of HOM Lorentzian dips. They can be viewed as the HOM noise correlation resulting from the collision at the QPC of two split Lorentzians LS1(t) and LS2(t-τ), with $LS1(t)=T_AL(t-L/v_2)+R_AL(t-L_A/v_2-(L-L_A)/v_1)$ and $LS2(t)=T_BL(t-L/v_4)+R_BL(t-L_B/v_4-(L-L_B)/v_3)$ where L(t) denotes the generic Lorentzian pulse sent to ohmic contacts and $v_{1(3)}$ denotes the velocity of the outer upper (lower) channels and $v_{2(4)}$ the velocities of the upper (lower) inner channels and L=20μm is the distance between the ohmic contacts and the QPC Eq. S7 justifies the generic form: $Cst + AS_{HOM}(\Delta_{13}) + BS_{HOM}(\Delta_{23}) + CS_{HOM}(\Delta_{14}) + DS_{HOM}(\Delta_{24})$ used to fit the ν=2 HOM noise data of figure 3(a) main text. For the fit of figure 3(a) we use $LS1(t)=0.66L(t)+0.33L(t-70ps)$ and $LS2(t)=0.45L(t-\tau_0)+0.55L(t-\tau_0-77ps)$ where $\tau_0$=20ps is an arbitrary time delay, known modulo the 200ps period, arising from propagation delays in the RF coaxial lines. From figure S1 we expect the distance of $L_A$ and $L_B$ to be about 16μm. The close 70 and 77ps values suggest a small left-right 1.6 μm asymmetry in the QPC gate location coming from device fabrication. A detailed study at ν=2 will be detailed in Ref.[51]. Note that the orders of magnitudes of the various time-delays are in the range expected for inner-outer edge velocities known to range between few $10^4$m/s and few $10^5$m/s, see Ref.[32,34,35]. The most important message of figure 3(a) is that the shape of the Lorentzian are unperturbed, in contrast to what is observed in figure 3(c) at ν=2/3.

**C2. HOM Shot noise at ν=2/3 using sinewave instead of Lorentzian pulses:**

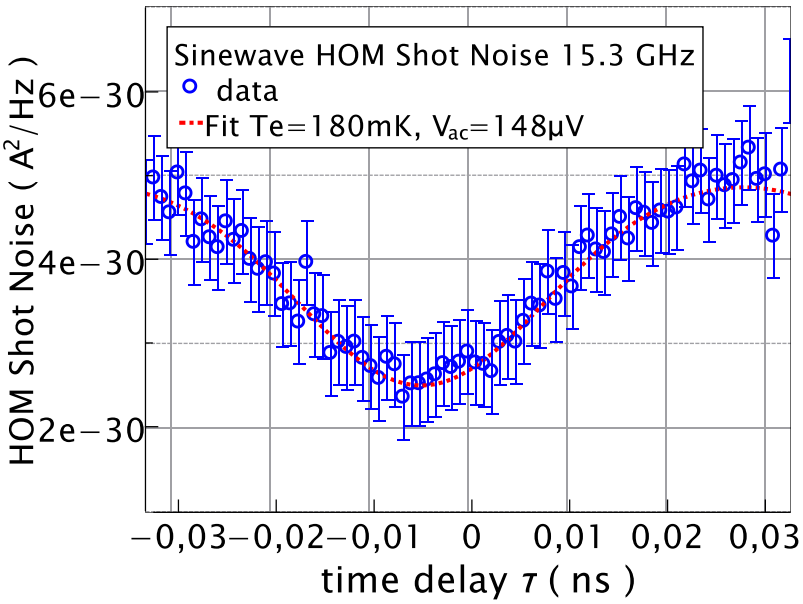


**Figure S8: HOM shot noise with sinewave at 2/3:** The blue open circle are the experimental data taken at base temperature with *f*=15.3GHz. The inner edge channel is weakly backscattered, 1-D=0.02. The red dashed line is a fit from equation (4) with Bessel function argument replaced by $(e^*/hf)2V_{ac}\sin(\pi f\tau)$ using an equal AC amplitude for right and left incoming voltage at the QPC of $V_{ac}$=148+/-3µV. A small noise offset of 2.5e-30$A^2$/Hz has been included in the fit. The $V_{ac}$ value is compatible with PASN measurements, giving 143+/-3µV and displayed in figure 2(b) of the main text.

In figure S8, we show that, injecting sinewave pulses instead of Lorentzian pulses on contact (1) and (2) at ν=2/3, gives a HOM analysis in excellent agreement with the analysis of independent PASN measurements, shown in Fig.2 main text, where the RF sinewave is injected to one contact only.

**Additional References:**


58. Palacios, J., J.& Tejedor, C., Effects of geometry on edge states in magnetic fields: Adiabatic and nonadiabatic behavior, Phys. Rev. B 45, 9059 (1992)

59. Pala, M. G., Governale, M., Zülicke, U., & Iannaccone, G., Rashba spin precession in quantum-Hall edge channels, Phys. Rev. B 71, 115306 (2005)

60. Müller, G., Weiss, D., Khaetskii, A., V., von Klitzing, K., Koch, S., Nickel, H., Schlapp, W., & Lösch, R., Equilibration length of electrons in spin-polarized edge channels, Phys. Rev. B 45, 3932(R) (1992)

61. Acremann, Y., Heinzel, T., Ensslin, K., Gini, E., Melchior, H., & Holland, M., Individual scatterers as microscopic origin of equilibration between spin-polarized edge channels in the quantum Hall regime, Phys. Rev. B 59, 2116 (1999)

62. Nicolí, G., et al, Spin-Selective Equilibration among Integer Quantum Hall Edge Channels, Phys. Rev. Lett. 128 056802 (2022)

63. Paradiso, N. et al., Spatially resolved analysis of edge-channel equilibration in quantum Hall circuits, Phys. Rev. B 83, 155305 (2011)